INL/CON-08-13801
PREPRINT

Numerical Prediction of the Performance of Integrated Planar Solid-Oxide Fuel Cells, With Comparisons of Results from Several Codes

6th International Conference on Fuel Cell Science, Engineering, and Technology

G. L. Hawkes
J. E. O'Brien
B. A. Haberman
A. J. Marquis
C. Martinez Baca
R. P. Travis
P. Costamagna
D. Tripepi

The INL is a
U.S. Department of Energy
National Laboratory
operated by
Battelle Energy Alliance

June 2008

Proceedings of FUELCELL2008:
6th International Conference on Fuel Cell Science, Engineering and Technology
June 16 – 18, 2008; Denver, CO

FUELCELL2008 - 65179

NUMERICAL PREDICTION OF THE PERFORMANCE OF INTEGRATED PLANAR SOLID-OXIDE FUEL CELLS, WITH COMPARISONS OF RESULTS FROM SEVERAL CODES

G. L. Hawkes, J. E. O'Brien
Idaho National Laboratory
Idaho Falls, ID, USA

B.A. Haberman, A. J. Marquis
Imperial College London
London, UK

C. Martinez Baca, R.P. Travis
Rolls-Royce Fuel Cell Systems Limited
Loughborough, UK

P. Costamagna, D. Tripepi
University of Genoa
Genoa, Italy

ABSTRACT

A numerical study of the thermal and electrochemical performance of a single-tube Integrated Planar Solid Oxide Fuel Cell (IP-SOFC) has been performed. Results obtained from two finite-volume computational fluid dynamics (CFD) codes FLUENT and SOHAB and from a two-dimensional in-house developed finite-volume GENOA model are presented and compared. Each tool uses physical and geometric models of differing complexity and comparisons are made to assess their relative merits. Several single-tube simulations were run using each code over a range of operating conditions. The results include polarization curves, distributions of local current density, composition and temperature. Comparisons of these results are discussed, along with their relationship to the respective imbedded phenomenological models for activation losses, fluid flow and mass transport in porous media. In general, agreement between the codes was within 15% for overall parameters such as operating voltage and maximum temperature. The CFD results clearly show the effects of internal structure on the distributions of gas flows and related quantities within the electrochemical cells.

INTRODUCTION

Integrated Planar Solid Oxide Fuel Cells (IP-SOFC) are currently under development for hybrid power applications [1,2]. A typical IP-SOFC consists of a flattened ceramic tube with segmented-in-series electrochemical cells deposited on its outer surfaces. This design concept represents a cross between tubular and planar fuel cell designs. Oxygen is supplied to the cathodes from air flowing over the outside of the tubes and hydrogen diffuses from the internal fuel channels to the anodes through the porous tube structure. The IP-SOFC is intended for use in medium-scale 1 MW stationary power applications. These systems will utilize fuel cell stacks containing many thousands of tubes housed inside a pressure vessel [3]. Modeling the gas flow, thermal and electrochemical behavior of these stacks is a critical part of the design process and in recent years several simulation tools have been developed specifically for this task [4-7]. The purpose of this study is to make a comparison between several of these tools, including: the three-dimensional finite-volume CFD codes FLUENT and SOHAB and the 2-D in-house developed finite-volume GENOA model.

NOMENCLATURE

d_p	pore diameter
h	thickness
i	current density
i_o	exchange current density
I	cell current
T	temperature
V	voltage
X_i	mole fraction of component i

IP-SOFC MODEL GEOMETRY

A single half-tube model was considered in this study, as shown in Fig. 1. The tube has 15 fuel flow channels and ten fuel cells printed on its outer surface. Adiabatic symmetry boundaries are assumed on the top and bottom external surfaces highlighted by broken lines in Fig. 1.

Fuel flow is introduced directly into the 15 channels as a mass-flow boundary condition at the lower left in Fig. 1. Air

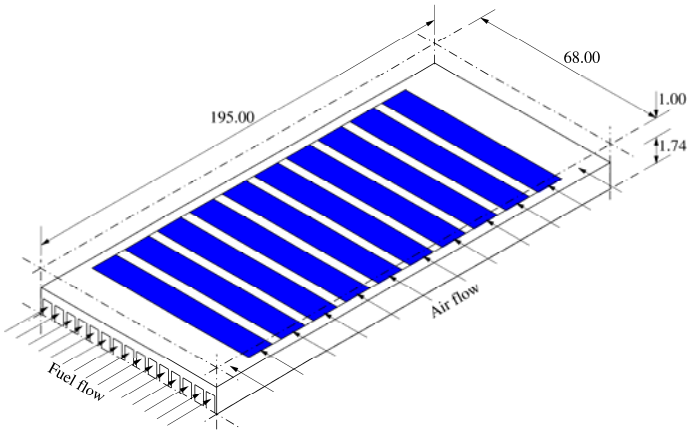

Figure 1. Single half-height tube model (dimensions in millimeters).

is introduced as a mass-flow boundary condition at the lower right. The air flow region extends 1.0 mm above the cells, representing half of the distance to the adjacent tube within a possible stack design. A cross-sectional view of the cell geometry is shown in Figure 2, based on typical public-domain data for a row of segmented-in-series cells [8].

Each cell comprises the anode, electrolyte and cathode layers and an additional layer, the cathode current collector (CCC), which is used to increase the electrical conductivity of the air side of the cells [8]. The properties of these cell components and the supporting tube are listed in Table 1 [8,9]. Constant exchange current densities i_0 have been specified to facilitate straightforward comparisons between models.

The prescribed pressure and temperature boundary conditions at the fuel and air flow inlets are 1 bar and 1173 K. Inlet compositions are 97% hydrogen and 3% steam in the fuel channels and 20% oxygen, 80% nitrogen on the air side. Inlet mass flow rates of 3.71 x 10^{-7} kg/s and 1.5 x 10^{-4} kg/s are specified for each of the fuel and air flow channels, respectively. Outlet pressures of 1 bar are prescribed for both

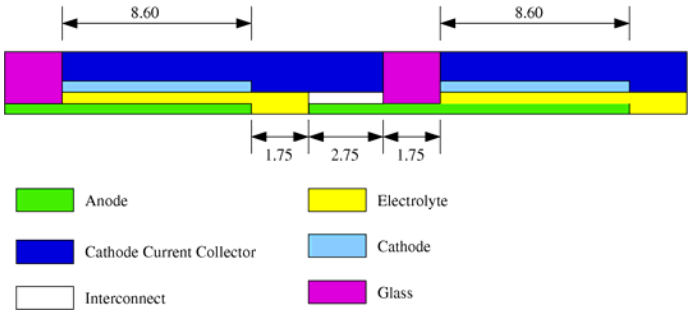

Figure 2. IP-SOFC cell layout and dimensions in millimetres.

the fuel and flows. The overall fuel utilization for an individual IP-SOFC tube is low (around 2.5% for a nominal operating current of 1.032 A) and within a stack the complete fuel flow path comprises several tubes connected in series.

COMPUTER CODES

This study compares the simulation results obtained from the IP-SOFC model described above using four computer codes: FLUENT-INL, FLUENT-RR, SOHAB and GENOA. The FLUENT-INL results were produced at the Idaho National Laboratory using version 6.3.26 of FLUENT. The FLUENT-RR results were produced at Rolls-Royce Fuel Cell Systems Limited using version 6.2.16 of FLUENT [10]. The newer version of the FLUENT SOFC module allows for more control over the parameters in the activation model. In particular, the concentration exponent in the expression for exchange current density can be specified [11]. The SOHAB results were produced at Imperial College based on a code developed by Haberman [9]. This code uses an explicit time marching scheme on structured rectangular grids and thus the computational domain for this study is split into a series of grids that communicate through their shared boundaries. This method is designed to simulate discontinuous computational domains such as the model used in this study. Finally, the

Table 1. IP-SOFC dimensions and properties.

Property	Tube Wall	Anode	Electrolyte	Cathode	CCC
Composition	-	YSZ-Ni	YSZ	YSZ-LSM	LSM
Porosity, ε	0.2	0.2	0	0.2	0.2
Tortuosity, β	2	2	0	2	2
Pore diameter, d_p (μm)	3	1	0	1	1
Thickness, h (μm)	800	30	20	30	175
Thermal conductivity, k (W/m·K)	5	5	5	5	5
Electrical conductivity σ_e(S/cm)	-	700	-	25	50
Ionic conductivity σ_i(S/cm)	-	-	0.14	-	-
Exchange current density, i_o (A/cm^2)	-	5300	-	2000	-

GENOA model is a 2-D model developed in-house at the University of Genoa. In this model, the IP-SOFC tube is simulated as a typical electrochemical reactor. In particular, the model is based on local balances of mass and energy, coupled to a suitable electro-kinetics subroutine [12]. The numerical solution is carried out through a finite volume method coupled to relaxation. The code is written in FORTRAN language.

The SOHAB numerical model included about 500,000 finite-volume cells, the FLUENT-INL model used 1.2 million cells, the FLUENT-RR model used 850,000 and the GENOA model employed about 450 grid cells. Experience shows that results should be very close for the Fluent-INL and Fluent-RR grids that are used. The FLUENT-SOFC module used by INL has been verified to be correct and gives temperature results within ~2.4% of older modules. Grid independence was verified with all models.

Based on all residuals decreasing by five orders of magnitude, SOHAB convergence was achieved after about 2500 time steps. For the FLUENT-INL runs, convergence was deemed acceptable after the continuity residual decreased to lower than 5×10^{-5}, which was generally achieved after about 55 iterations. The continuity residual was chosen since it is always the highest and slowest to converge. The convergence of the GENOA code is based on a relaxation method which follows a fictitious transient of the solid temperature distribution over the tube. Convergence is reached when temperatures change less than 5.5×10^{-5} % per second of simulated time. This is generally achieved after 300,000 iterations.

FLUENT-INL was run on a single-CPU 2.6-GHz machine running SUSE 10.0 Linux. Each run required about 53 minutes of real time. SOHAB was run on a 2.4 GHz AMD dual core Opteron processors, also running SUSE 10.0 Linux. With two processor cores, each run required about 46 minutes of real time. The GENOA codes runs on a PC with 1.50 GHz Intel Pentium M single processor, with Windows XP operating system. Each run required a couple of minutes of real time.

OVERALL RESULTS

Overall results obtained from the single-tube simulations are summarized by Table 2 and Fig. 3. Table 2 indicates the hydrogen and oxygen consumption rates over a range of currents drawn through the cells. These rates are calculated from mass-averaged summations at the inlet and outlets of the model. It is also possible to calculate conservation errors for each variable by comparing these numerical predictions against theoretical global conservation calculations, also listed in the table. Conservation errors for hydrogen consumption are provided in Table 2 based on the SOHAB and FLUENT-INL results. These errors were very small (<0.07%) for the FLUENT results and a bit larger (<0.27%) for the SOHAB results. In general, both codes achieve acceptable levels of accuracy for all conserved variables. For the specified fuel flow rate, the per-tube fuel utilization value corresponding to the maximum current of 3.096 A was only 7.7%.

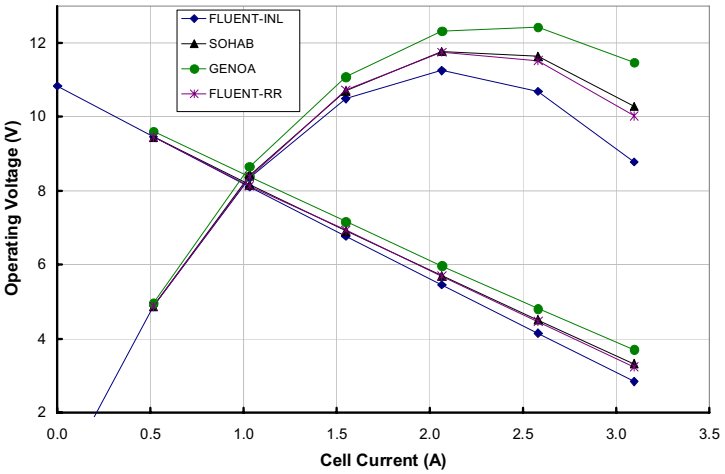

Figure 3. Polarization and power curves.

Tube operating voltages and power output values are presented in Fig. 3 over a range of total cell current values from 0.0 to 3.096 A. The per-cell active area is 5.16 cm^2, so the maximum current corresponds to a current density of 0.6 A/cm^2. Operating voltage decreases nearly linearly from an open-cell value of 10.83 V to ~3 V at the maximum current. The GENOA model predicted the highest tube operating voltages and tube power output. The FLUENT-INL model

Table 2. Hydrogen and Oxygen consumption rates.

Cell Current (A)	H_2 Consumption (kg/s)					O_2 Consumption (kg/s)		
	Theoretical	SOHAB	FLUENT	% difference SOHAB	% difference FLUENT	Theoretical	SOHAB	FLUENT
0.516	5.391×10^{-8}	5.397×10^{-8}	5.391×10^{-8}	0.12	0.0138	4.278×10^{-7}	4.270×10^{-7}	4.278×10^{-7}
1.032	1.078×10^{-7}	1.079×10^{-7}	1.078×10^{-7}	0.11	0.0214	8.557×10^{-7}	8.540×10^{-7}	8.556×10^{-7}
1.548	1.617×10^{-7}	1.619×10^{-7}	1.618×10^{-7}	0.14	0.0318	1.284×10^{-6}	1.282×10^{-6}	1.283×10^{-6}
2.064	2.156×10^{-7}	2.160×10^{-7}	2.157×10^{-7}	0.18	0.0438	1.711×10^{-6}	1.710×10^{-6}	1.711×10^{-6}
2.580	2.695×10^{-7}	2.701×10^{-7}	2.697×10^{-7}	0.22	0.0562	2.139×10^{-6}	2.138×10^{-6}	2.139×10^{-6}
3.096	3.235×10^{-7}	3.243×10^{-7}	3.237×10^{-7}	0.27	0.0679	2.567×10^{-6}	2.566×10^{-6}	2.567×10^{-6}

predicted the lowest operating voltages and output power values. Peak output power values were in the 11 – 12 W range, occurring at ~2.5 A, or at a current density of 0.48 A/cm^2. These differences are related to choice of physical models within each code.

On the one hand, the FLUENT and SOHAB models differ in their treatment of the flow in porous media and activation overpotential. On the other hand, the main difference between the CFD codes and the GENOA model is that the latter is essentially a 2-D model (*x-y* tube plane), and the phenomena occurring along the tube thickness (heat and mass transfer) are treated in a simplified manner.

DETAILED SIMULATION RESULTS

Detailed results for distributions of temperature, mole fraction, and current density are presented in Figs. 4 – 12 for the base-case total current value of 1.032 A, corresponding to a current density of 0.2 A/cm^2. Contour plots of temperatures on the top surface of the ceramic support tube are presented in Fig. 4, based on the FLUENT, SOHAB, and GENOA results. The black rectangular outlines in Figs. 4(a) and 4(b) represent the locations of the individual cells. The dotted lines in Fig. 4(b) represent the locations of the individual fuel-channel walls. The inlet temperature for both the fuel and the air is 1173 K. Fuel enters the domain from the left and air enters from the bottom. Maximum temperatures occur in the upper right of the figures, corresponding to the outlet side for both the fuel flow and the air flow. Heating is caused by the exothermic electrochemical reaction and also from cell irreversibilities, such as electric and ionic resistance, activation, and concentration polarization. Predicted maximum temperatures are highest for the FLUENT-RR results, followed by the SOHAB results. Maximum temperatures predicted by the FLUENT-INL results and the GENOA results are very close. The shapes of the temperature distributions are remarkably similar among the four sets of results.

Radiation heat exchange has been neglected for the single tube calculations presented here because the view factors between axial locations along the length of the internal fuel flow channels are small. It should be noted that these temperature distributions do not provide a realistic representation of stack operation because the effect of the surrounding tubes has been neglected and radiation will be a significant form of heat transfer in this case.

Temperature contours in the *x-z* midplane (side view of the tube) are presented in Fig. 5 based on the FLUENT-INL (a) and SOHAB (b) results. These figures are presented with a vertical exaggeration factor of 35. Temperatures in the fuel

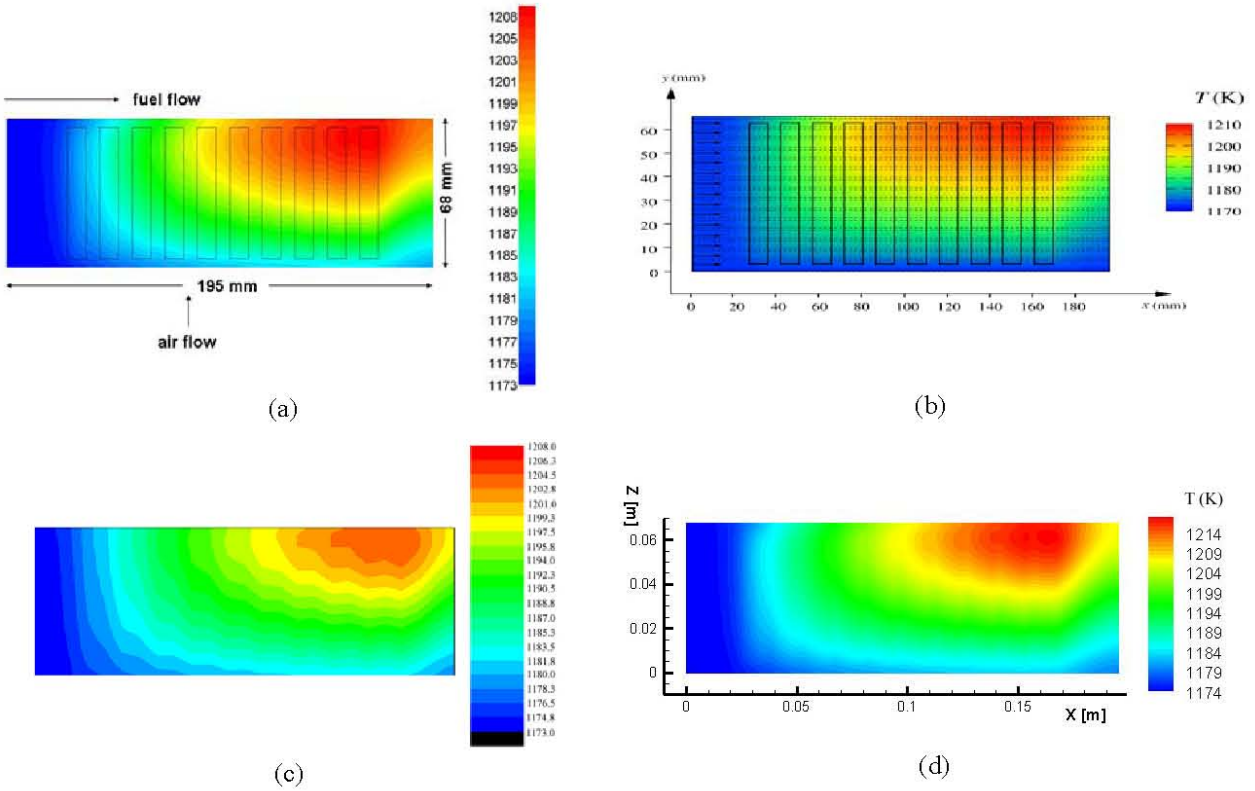

Figure 4. Top view of temperature contours on ceramic tube; (a) FLUENT-INL, (b) SOHAB, (c) GENOA, (d) FLUENT-RR.

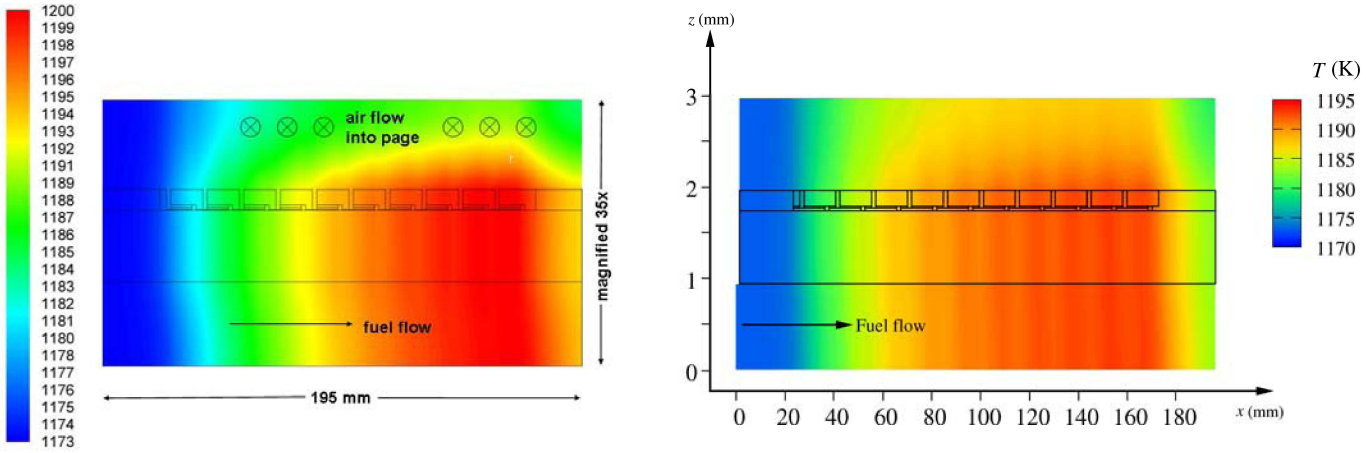

(a) (b)

Figure 5. Side view (*x*-*z* midplane) of temperature distributions; (a) FLUENT-INL, (b) SOHAB

flow channel are visible in the bottom portion of the figures, increasing from left to right. The middle portion of the figure represents the support structure, with the cell layers printed on top face. The upper portion of the figures represents the air flow region. The air flow direction is into the page. Adiabatic symmetry boundaries are specified at the bottom and top of these domains. The FLUENT-INL results indicate a more significant effect of advection in the fuel flow channel compared to the SOHAB results.

Although the variations of temperature in the *z*-direction are small, they have a significant effect on the conduction of heat between the fuel and air flows and hence on the temperature distribution throughout the tube. These results highlight the dependence of the temperature field on the direct thermal connection between the air and fuel flows. In contrast, no direct physical connection exists for the actual air and fuel gases (i.e., no mixing); therefore, the distributions of gas composition are quite different.

Distributions of hydrogen mole fraction in the *x*-*z* midplane are presented in Fig. 6, again with a vertical exaggeration factor of 35. These figures indicate the general decrease in hydrogen mole fraction in the fuel flow direction as hydrogen is consumed by the electrochemical reaction. The figures also indicate a vertical gradient of hydrogen mole fraction associated with the migration of hydrogen toward the individual cells through the porous ceramic support tube structure. These vertical gradients and internal wall surfaces are much more pronounced in the SOHAB results compared to the FLUENT results, despite both codes using a similar grid refinement of three cells evenly spaced through the thickness of the electrodes.

The differences in calculation results can be attributed to the different physical modeling approaches utilized. The SOHAB code models distinct boundaries between porous and

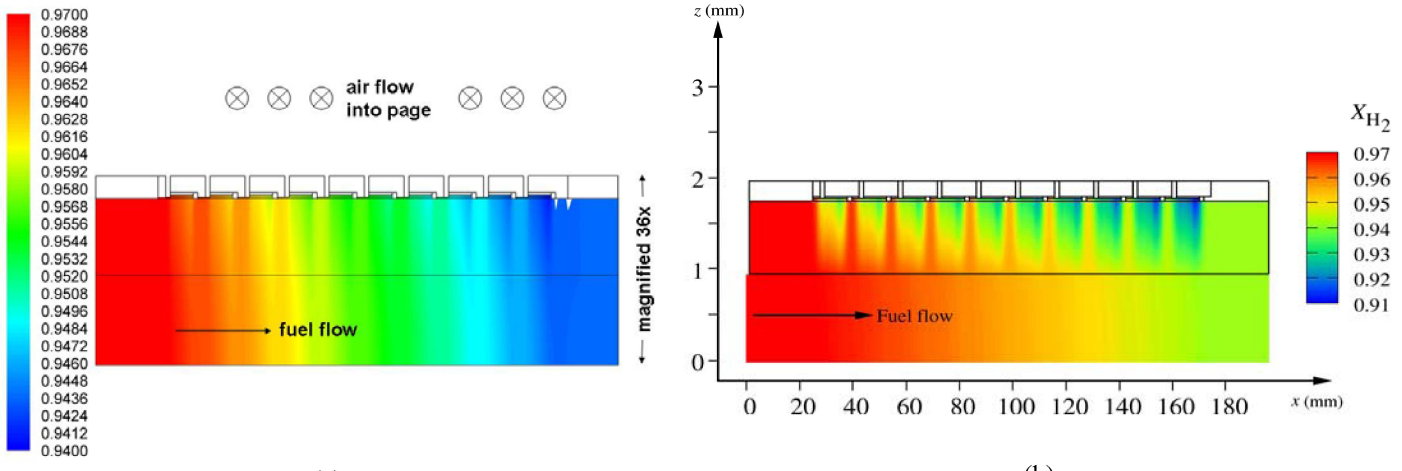

(a) (b)

Figure 6. Side view (x-z midplane) of hydrogen mole fraction distributions; (a) FLUENT-INL, (b) SOHAB.

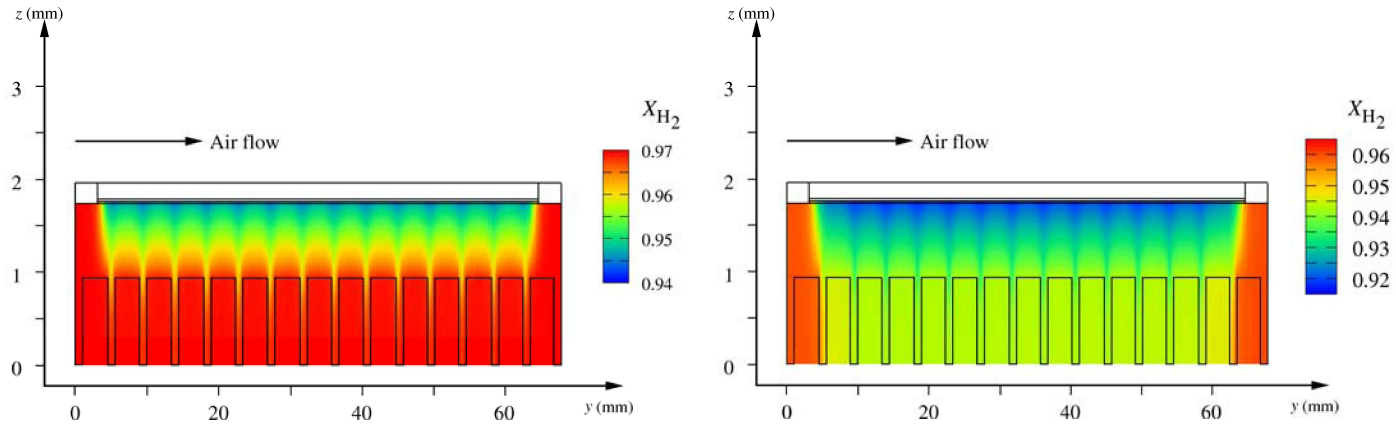

Figure 7. Cross-sectional views (*y*-*z* plane) of hydrogen mole fraction distributions (SOHAB); (a) x =32 mm, (b) x = 164 mm

gaseous regions and also employs the more fundamental Cylindrical Pore Interpolation Model that provides a complete description of the reactive flow in porous media [13]. The FLUENT-SOFC module utilizes the core FLUENT model for mass diffusion which is based on the Maxwell-Stefan equations. In the FLUENT-SOFC module the diffusion coefficient is multiplied by the ratio of porosity divided by tortuosity to account for the effect of the porous electrodes. The electrochemically inactive regions near the fuel inlet and outlet are evident in the figure.

Cross-sectional views of the distribution of hydrogen mole fraction at two locations along the fuel flow direction are presented in Figs. 7 and 8, based on simulations performed with SOHAB and FLUENT respectively. A vertical exaggeration factor of 35 was again used in preparing these figures. The outlines of the individual flow channels are shown in the figures. These distributions are virtually symmetric about the y = 34 mm midplane, despite the cross-flow of air. The effect of the 15 individual fuel channel walls is clearly reflected in the periodicity of the mole-fraction distributions in the y-direction. A comparison of the distributions at x = 32 mm and x = 164 mm shows that as fuel flows along the length of the tube a mole-fraction gradient develops between the fuel-rich outermost channels and their neighbors, which causes hydrogen to diffuse in the *y*-direction towards the centre of the tube. Thus the distribution of X_{H2} is fundamentally three-dimensional and hydrogen is consumed, to some degree, from all of the fuel channels.

A Comparison between Figs. 7 and 8 highlights the differences between the models used by the SOHAB and FLUENT codes to describe mass transport in porous materials. The SOHAB code predicts larger variations in hydrogen mole fraction in the porous regions of the tube than FLUENT and this is especially evident in the fuel channels and their adjacent walls. The variations in the *y*-direction predicted by the SOHAB code are confined to the tube walls whereas FLUENT

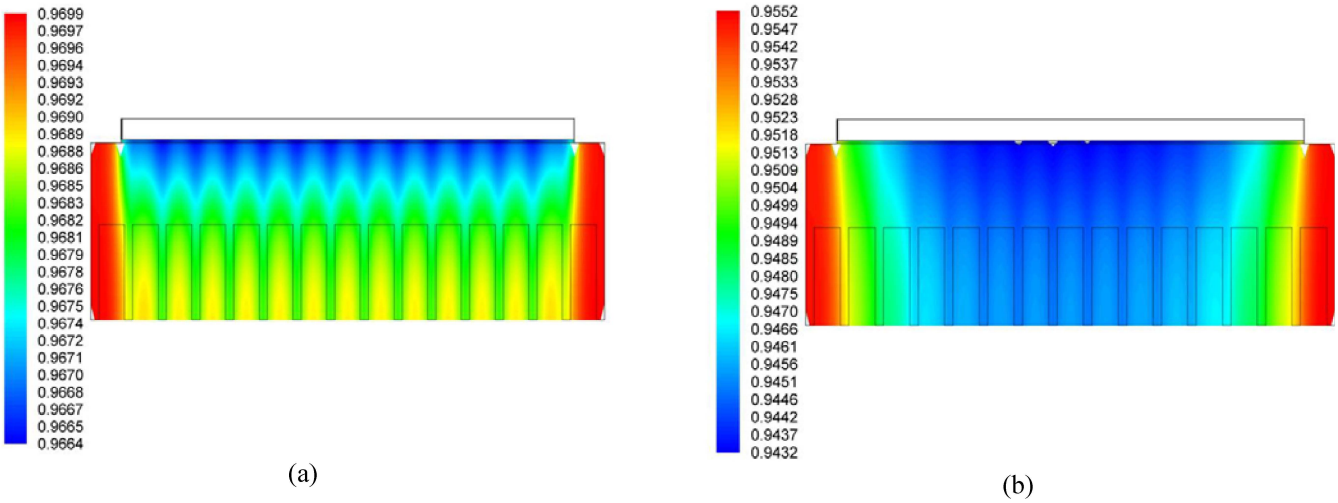

Figure 8. Cross-sectional views (*y*-*z* plane) of hydrogen mole fraction distributions (FLUENT-INL); (a) x =32 mm, (b) x = 164mm.

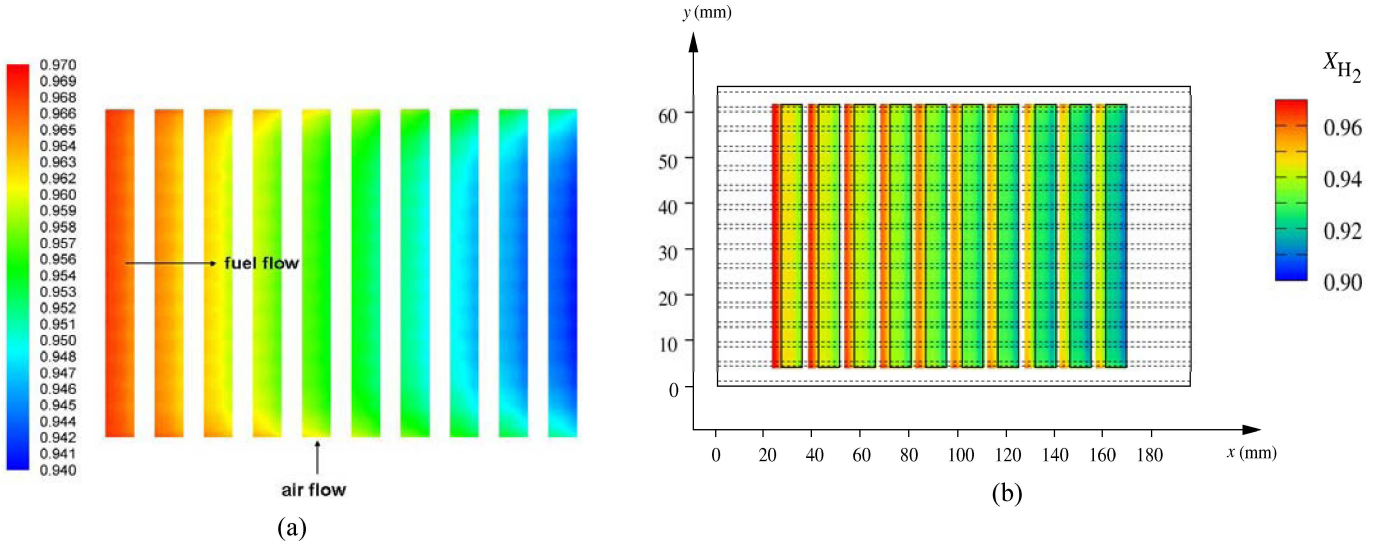

Figure 9. Top view (x-y plane) of hydrogen mole fraction distributions at the anode/electrolyte interface; (a) FLUENT-INL, (b) SOHAB.

predicts similar magnitude variations across the both the fuel channels and their adjacent walls.

Top views of hydrogen mole fraction distributions at the anode/electrolyte interface are presented in Fig. 9, with a vertical exaggeration factor of 2. Fig. 9 (a) does not include the regions between the cells. Figure 9 confirms that X_{H2} decreases in successive cells in the fuel flow direction. On close inspection, the fuel conditions are slightly richer in hydrogen at y = 4mm and y = 64 mm due to proximity to the outermost fuel channels at these locations. The effects of the individual fuel flow channels can again be observed in this view. The fuel cells are more deprived of fuel in the regions directly above fuel channel walls where the fuel flow path is slightly longer.

Similarly, the distribution of X_{O2} is also influenced by the tube geometry and gas flow. Figure 10 shows this distribution plotted in the x-y plane located at the cathode/electrolyte interface. Since the results presented in Fig. 10(a) do not include the relatively unaffected regions of air flow between the cells, its range of displayed mole fraction values is much tighter than in Fig. 10(b). Fig. 10(a) clearly shows that air-side surface oxygen mole fractions decrease in the air flow direction, more rapidly on the downstream side of each cell, with respect to the fuel flow direction. As we shall see, this is a consequence of the non-uniform local current density distribution, with higher current densities toward the

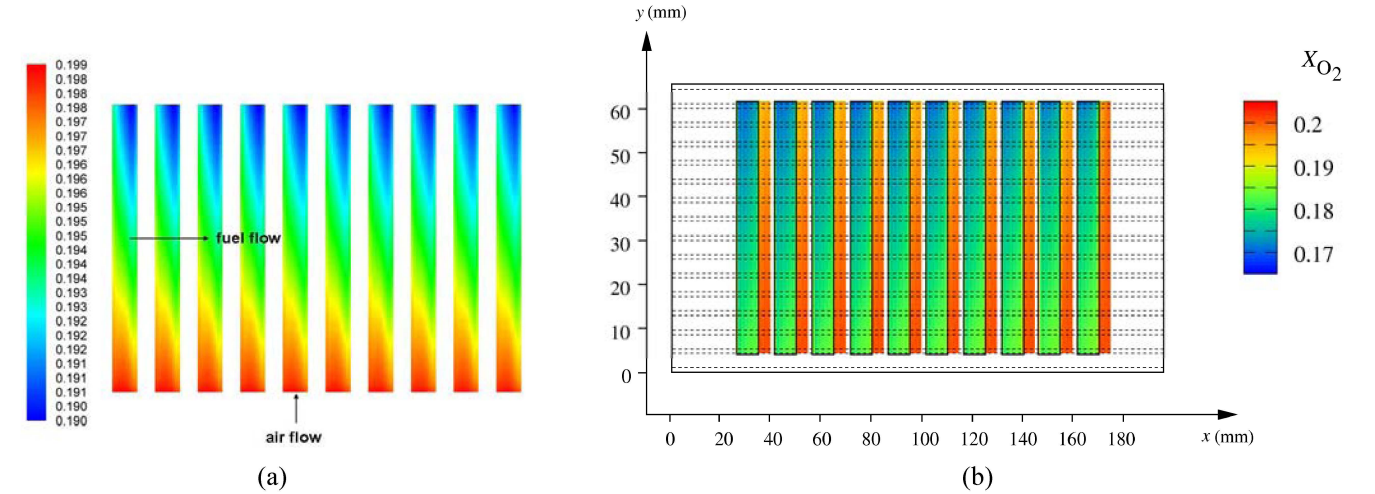

Figure 10. Top view (x-y plane) of oxygen mole fraction distributions at the cathode/electrolyte interface; (a) FLUENT-INL, (b) SOHAB.

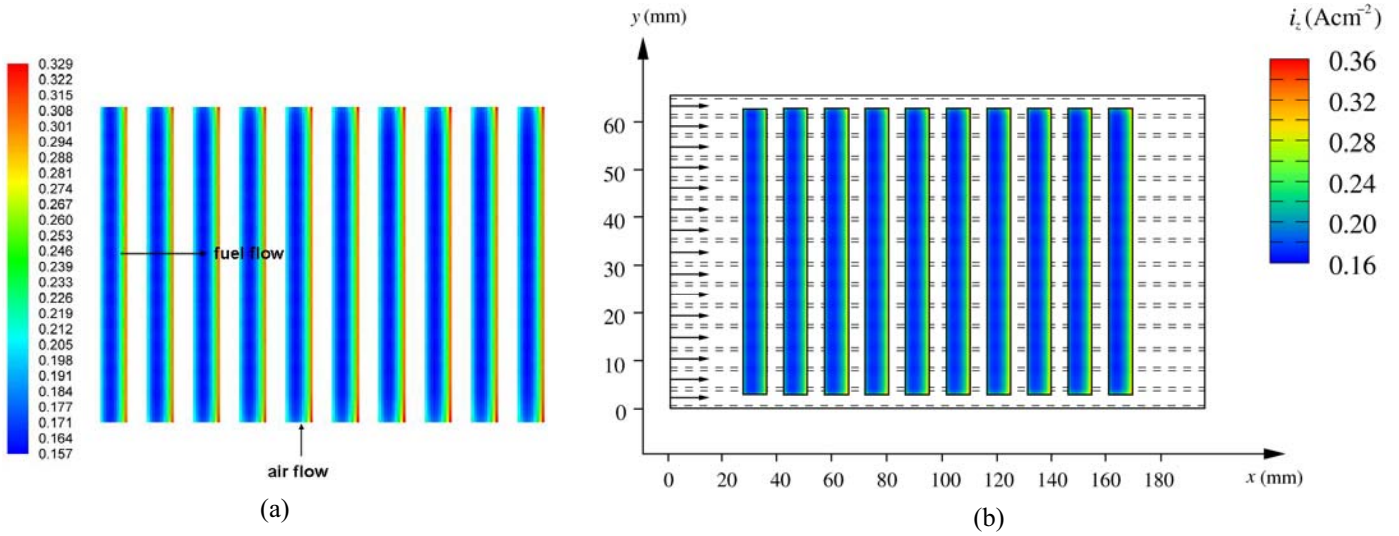

Figure 11. Top view (*x*-*y* plane) of conventional (*z*-direction) electrolyte current density distributions; (a) FLUENT-INL, (b) SOHAB.

downstream side of each cell.

Figure 11 shows a top view of the local conventional (*z*-direction) current density i_z flowing through the electrolyte in the *x*-*y* plane. The magnitude of the current density varies primarily in the *x*-direction only, with the highest values near the downstream edge of each cell with respect to the fuel flow direction. In general, current flow is biased towards the right hand side of each electrolyte as it follows the path of least resistance and flows preferentially in the higher conductivity anode. Also, the electrolyte current density i_z is slightly promoted in regions directly above fuel channels where the fuel flow path length is minimized and concentration losses are smallest. A comparison between the i_z distributions calculated for successive cells in the *x*-direction highlights the influence of the changing gas conditions presented in previous figures. The first cell (located at x = 35 mm, in close proximity to the fuel inlets) experiences almost uniform gas conditions and hence shows little i_z variation in the *y*-direction. However, as conventional current flows on to successive cells and the gas properties start to show some variation, i_z is promoted in regions adjacent to the outermost fuel channels (y = 4mm and y = 64 mm) where the gas conditions are richer in fuel.

A line plot of midplane conventional current densities is presented in Fig. 12 for two values of total current, 1.032 A and 2.064 A, based on the FLUENT-INL simulations. This plot shows that the highest current densities occur near the upstream and downstream edges of the cells, with respect to the fuel flow direction. The magnitude of the maximum-to-minimum current density ratio is nearly a factor of two.

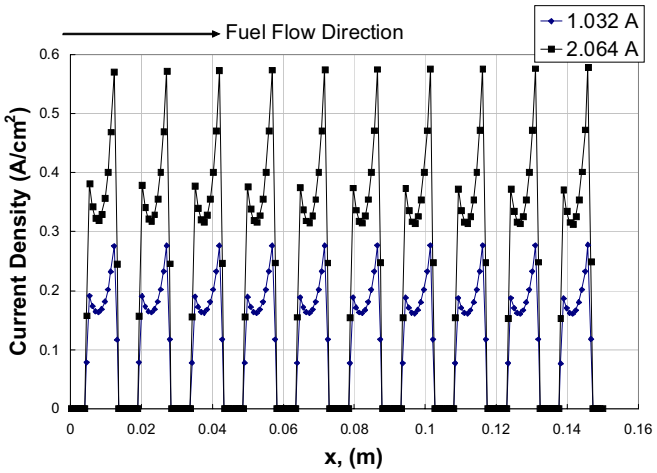

Figure 12. Midplane (y = 34 mm) variation in electrolyte current density, based on FLUENT-INL simulations.

CONCLUSIONS

The development of computer simulation tools for SOFC applications requires an understanding of a range of physical processes including: current flow, mass transport in porous media, fluid flows and electrochemistry. A comparison has been made between the results obtained from several of these tools; the SOHAB and FLUENT three-dimensional finite volume CFD codes and the two-dimensional in-house developed finite-volume GENOA code. A model of a single IP-SOFC tube consisting of 10 segmented-in-series cells fabricated onto a flattened porous support tube was used for the comparison.

Typically, the CFD codes required about 1 hour to produce high resolution results from models consisting of 500,000 – 1,000,000 computational grid cells whereas the GENOA code produced a coarser result from a model containing about 450 grid cells in a few minutes. Overall, good agreement was obtained for global parameters such as electrical power output

and fuel utilization, despite the variety of different numerical techniques and physical models being utilized. Overall the fuel utilization within a single IP-SOFC tube is low because complete fuel flow path within a stack comprises several tubes connected in series.

More detailed comparisons were also made between the predicted distributions of gas properties and current densities within the tube, at a nominal operating current. Here the differences between the results became more apparent; most notably in the porous regions of the tube where a range of mass transport and geometric models are used. This level of resolution is beyond the remit of the GENOA code which has been designed for fast computational speed and is suitable to be integrated into system simulations.

All the cases examined in this study represent hydrogen with steam at atmospheric pressure. Modes of operation for SOFCs include other fuels and higher pressures see for example [1], and future work will include this investigation. This comparison work is an important part of code development and will be used to further improve the methods presented in this study.

ACKNOWLEDGMENTS

The work performed at INL was supported by the US Department of Energy, under the Nuclear Hydrogen Initiative. The work performed at Imperial College and Genoa University was financially supported by Rolls-Royce Fuel Cell Systems Limited Research Grants.

REFERENCES

1. Agnew, G. D., Bozzolo, M., Moritz, R. R., and Berenyi, S., "The Design and Integration of the Rolls-Royce Fuel Cell System 1 MW SOFC," Proceedings of the ASME Turbo Expo., Vol. 2, pp. 801 – 806, 2005.

2. Agnew, G.D., Collins, R.D., Jorger, M., Pyke, S.H., and Travis, R.P., The Components of a 1MW SOFC System at Rolls-Royce, Transactions of the ECS, Volume 7, 2007.

3. Magistri, L., Bozzolo, M., Tarnowski, O., Agnew, G. D., and Massardo, A. F., "Design and Off-design Analysis of a MW Hybrid System based on Rolls-Royce Integrated Planar Solid Oxide Fuel Cells," *Journal of Engineering for Gas Turbines and Power*, Vol. 129, no. 3, pp. 792-797, 2007.

4. Costamagna, P. Selimovic, A. Borghi, M. D., and Agnew, G., "Electrochemical Model of the Integrated Planar Solid Oxide Fuel Cell (IP-SOFC)," *Chemical Engineering Journal*, Vol. 102, pp. 61-69, 2004.

5. Cannarozzo, M., Grosso, S., Agnew, G. D., Del Borghi, A., and Costamagna, P., "Effects of Mass Transport on the Performance of Solid Oxide Fuel Cells Composite Electrodes," *Journal of Fuel Cell Science and Technology*, Vol. 4, No. 1, pp. 99 – 106, 2007.

6. Haberman, B. A., and Young, J. B., "Numerical Investigation of the Air flow through a Bundle of IP-SOFC Modules," *Int. Journal of Heat and Mass Transfer*, Vol. 48, no. 25-26, pp.5475 – 5487, 2005.

7. Hawkes, G. L., O'Brien, J. E., and Stoots, C. M., "3D CFD Model of a Multi-Cell High Temperature Electrolysis Stack, paper 412e, Proceedings, 2007 AIChE Annual Meeting, Salt Lake City, November 4 – 9, 2007.

8. Lai, T. S. and Barnett, S. A., "Effect of cathode sheet resistance on segmented-in-series SOFC power density," *J. Power Sources*, Vol. 164, pp. 742-745, 2007.

9. Haberman, B. A. and Young J. B., "A Detailed Three-Dimensional Simulation of an IP-SOFC stack," *Journal of Fuel Cell Science and Technology*, Vol. 5, No. 1, 2008.

10. Bernardi, D., Tripepi, D., Massardo, A.F., Experimentally validated CFD model of an Integrated Planar Solid Oxide Fuel Cell, 5th Int Conf Fuel Cell Sci & Engg, New York, ASME, 2007.

11. Prinkey, M., Shahnam, M., and Rogers, W. "FLUENT 6.3 Fuel Cell Modules Manual," September, 2006.

12. Magistri, L., Traverso, A., Cerutti F., Bozzolo, M., Costamagna, P., and Massardo, A.F., "Modelling of Pressurised Hybrid Systems based on Integrated Planar Solid Oxide Fuel Cell (IP-SOFC) Technology", *Fuel Cells – From Fundamentals to Systems*, Vol. 5, no. 1, pp. 80-96, 2005.

13. Haberman, B. A., and Young, J. B., "Three-dimensional simulation of chemically reacting gas flows in the porous support structure of an integrated-planar solid oxide fuel cell," *Int. Journal of Heat and Mass Transfer*, Vol. 47, pp. 3617-3629, 2004.